POLİTEKNİK DERGİSİ

JOURNAL of POLYTECHNIC

ISSN: 1302-0900 (PRINT), ISSN: 2147-9429 (ONLINE)
URL: http://dergipark.org.tr/politeknik

Determination of subsurface thermoelastic contact stresses in a half-plane using temperature dependent properties

Bir yarı-düzlemde termoelastik temas gerilmelerinin sıcaklık bağımlı özellikler kullanılarak belirlenmesi

***Yazar(lar) (Author(s))**: Mehmet Nurullah BALCİ[1]*

ORCID[1]: 0000-0002-4416-6761

Bu makaleye şu şekilde atıfta bulunabilirsiniz(To cite to this article): Balci M.N., "Determination of subsurface thermoelastic contact stresses in a half-plane using temperature dependent properties", ***Politeknik Dergisi***, 25(1):257-272,(2022).

Erişim linki (To link to this article): http://dergipark.org.tr/politeknik/archive

DOI: **10.2339/politeknik.667386**

Determination of Subsurface Thermoelastic Contact Stresses in a Half-Plane Using Temperature Dependent Properties

Highlights

- *Contact mechanics between a rigid non-conductive punch and isotropic homogenous half-plane is carried out considering frictional heat generation.*
- *Frictional heat on the contact surface leads to temperature rise around contact region.*
- *Subsurface stresses are calculated based on the use of temperature dependent and temperature independent properties.*
- *Direct comparisons indicate that the utilization of temperature dependent properties is significant for accurate estimation of subsurface stresses especially at cases where higher values of sliding velocity and coefficient of friction exist.*

Graphical Abstract

Sliding contact mechanics problem between a rigid punch and homogenous isotropic half-plane is carried out considering frictional heat generation.

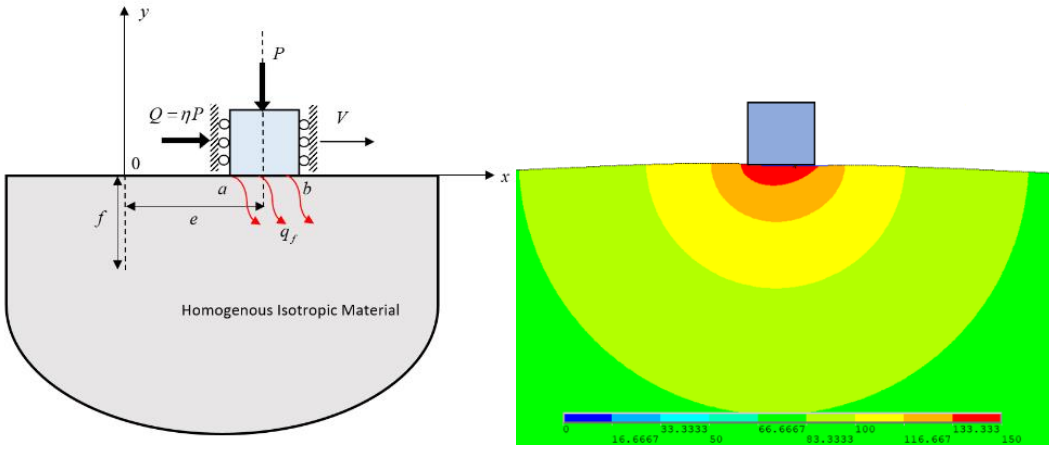

Figure. Schematics of the contact problem with frictional heat generation and temperature distribution around contact region

Aim

The main aim of this study is to investigate the influence of the utilization of temperature dependent material properties on subsurface contact stress distributions within the half-plane material.

Design & Methodology

An iterative algorithm is developed based on the finite element method. Thermal and structural analyses are performed sequentially until the frictional heat on the contact surface reaches equilibrium.

Originality

The main novelty of this study is to find the effect of the use of temperature dependent material properties on subsurface stresses in an elastic solid subjected to thermoelastic contact.

Findings

Increase in punch velocity and coefficient of friction leads to generation of greater heat on the contact surface.

Conclusion

The maximum percent difference between normal stresses is observed just below the contact surface $-1 \leq r \leq -0.9$ *while the maximum difference between subsurface shear stresses is seen around* $r \geq -0.9$. *Percent difference between subsurface stresses is higher both in front of the leading end and close vicinity of the contact.*

Declaration of Ethical Standards

The author(s) of this article declare that the materials and methods used in this study do not require ethical committee permission and/or legal-special permission.

Determination of Subsurface Thermoelastic Contact Stresses in a Half-Plane Using Temperature Dependent Properties

Araştırma Makalesi / Research Article

Mehmet Nurullah BALCİ*

Department of Mechanical Engineering, Hacettepe University, Ankara, Turkey

(Geliş/Received : 30.12.2019 ; Kabul/Accepted : 15.12.2020 ; Erken Görünüm/Early View : 02.01.2021)

ABSTRACT

Contact mechanics problem between a rigid punch and a homogenous half-plane is examined considering frictional heat generation. Friction between the sliding rigid punch and the surface of the half-plane leads to a frictional heat which directly flows towards the half-plane material without a loss, and it changes the material's thermoelastic properties. Calculation of subsurface stresses is crucial in the aspect of mechanical design of components since most of failures arise from fatigue and fracture at regions where subsurface stresses reach higher levels. In order to solve the problem, an iterative algorithm is developed based on the finite element method. Steady state subsurface contact stresses are obtained once the frictional heat on the contact surface reaches equilibrium. Subsurface stresses are calculated for different values of punch sliding velocity and coefficient of friction. It is observed that difference between subsurface contact stresses calculated based on temperature dependent and temperature independent properties is remarkable. Higher values of punch velocity and coefficient of friction leads to greater amount of heat generation, and percent difference between stresses reaches significant level especially near the contact surface. The utilization of temperature dependent material properties provides better approximation in assessing fatigue and fracture behavior of machine parts subjected to frictional contact with heat generation.

Keywords: Contact mechanics, friction, heat generation, subsurface stress, finite element analysis.

Bir Yarı-düzlemde Yüzeyaltı Termoelastik Temas Gerilmelerinin Sıcaklık Bağımlı Özellikler Kullanılarak Belirlenmesi

ÖZ

Rijit bir zımba ile homojen bir yarı-düzlem arasındaki temas mekaniği sürtünme ısı üretimi düşünülerek incelenmiştir. Kayan rijit zımba ile yarı-düzlem yüzeyi arasındaki sürtünme yarı-düzlem malzemeye doğru kayıp olmadan akan bir sürtünme ısısına yol acar, ve bu malzemenin termoelastik özelliklerini değiştirir. Yüzey altı gerilmelerin hesaplanması bileşenlerin mekanik tasarımı açısından çok önemlidir çünkü hasarların çoğu yüzey altı gerilmelerin daha yüksek seviyelere ulaştığı bölgelerdeki yorulma ve kırılmadan kaynaklanmaktadir. Problemi çözmek için sonlu elemanlar yöntemine dayanan iteratif bir algoritma geliştirilmiştir. Kararlı durum yüzey altı temas gerilmeleri temas yüzeyindeki sürtünme ısısı dengeye ulaştığında elde edilir. Yüzeyaltı temas gerilmeleri zımba kayma hızının ve sürtünme katsayısının çeşitli değerleri için elde edilmiştir. Sıcaklığa bağlı ve sıcaklıktan bağımsız özelliklere göre hesaplanan yüzey altı temas gerilmeleri arasındaki farkın dikkat çekici olduğu görülmektedir. Daha yüksek zımba hızı ve sürtünme katsayısı değerleri daha fazla miktarda ısı oluşumuna neden olur ve gerilmeler arasındaki yüzde fark özellikle temas bölgesinin yakınında önemli seviyeye ulaşır. Sıcaklığa bağlı malzeme özelliklerinin kullanılması, ısı üretimi ile sürtünme temasına maruz kalan makine parçalarının yorulma ve kırılma davranışının değerlendirilmesinde daha iyi bir yaklaşım sağlar.

Anahtar Kelimeler: Temas mekaniği, sürtünme, ısı üretimi, yüzeyaltı gerilme, sonlu elemanlar analizi.

1. INTRODUCTION

Contact mechanics analysis of solid bodies has always been an important topic to estimate wear, fatigue and failure mechanisms of machine components. Assemblages such as bearings, cams, cutting tools, gears and piston linings involve machine parts where friction mainly exists among them. Research on contact mechanics began in 1881 with studies carried out by Hertz [1]. Contact mechanics has been an attractive topic for scientists since it is directly pertaining to the surface wear, corrosion, durability and fatigue life of machine components. Johnson [2] provided some benchmark solutions to the contact problems involving elastic half-planes under different types of load. Frictional heat is one of the crucial parameters for contact mechanics analysis. Jaeger [3] studied sliding contacts, temperature distribution in the solid and author modelled heat as a moving source. Some thermoelastic contact problems

*Sorumlu Yazar (Corresponding Author)
e-posta : mehmetbalci@hacettepe.edu.tr

with frictional heat generation was examined analytically by Barber [4] and solutions for axisymmetric, sphere/plane and cylindrical/plane types of contact were provided by assuming one of the bodies as insulated. Dundurs and Comninou [5] utilized Green's functions to formulate exterior thermoelastic contact problems, analytically. Furthermore, contact mechanics with heat conduction effect was investigated in [6-9].

Barber and Martin-Moran [10] used Green's functions to solve thermoelastic contact problems in transient case. Hills and Barber [11] carried out an analytical study to solve the contact problem between a metallic half-plane and a rigid insulating punch considering frictional heat generation. Coulomb's friction law was adopted, and stress and temperature distributions were presented for various dimensionless parameters. Kulchytsky-Zhyhailo and Yevtushenko [12] developed an approximate method for the analysis of the temperature and pressure in an elastic layered medium due to frictional contact load. Authors utilized Fourier transformation method to solve the thermoelastic contact problem with frictional heat generation. Chao and Gao [13] used analytical continuation to solve the thermoelastic contact problem of homogenous half-plane indented by a rigid punch possessing different profiles. It was reported that separation could happen at the corners of the punch at critical sliding speed and it made the problem more complicated. Frictional contact problems involving heat generation due to the friction in stationary, quasi-stationary and non-stationary cases were studied by Matysiak and Yevthusenko [14]. Guler and Erdogan [15-16] solved contact mechanics problem of functionally graded material (FGM) coatings subjected to frictional contact by rigid punches possessing different shapes. Dag and Erdogan [17] analytically examined the coupled contact and a surface crack problem based on singular integral equation (SIE) technique. Ke and Wang [18-19] developed analytical method based on a singular integral equation for the solution of sliding contact problems of FGMs.

In the foregoing paragraph, some studies pertaining to frictional contact mechanics were mentioned and these studies utilized analytical approach for the solution of stress field in contact problems. However, not only analytical but also experimental or finite element methods can be used to compute surface contact or subsurface stresses in elastic solids under contact loads. Shi et al. [20] conducted an experimental study on the examination of polymer materials for bearings since these materials have some benefits over ordinary metals in view of lightweight, non-electric, chemical corrosion resistance and low cost. It was reported that the damage of polymer bearings under the contact load mainly due to the growth of subsurface cracks. Hence, determination of subsurface stress distribution is critical to understand the crack growth and the fatigue behavior. The subsurface microcracks due to the maximum shear stress leads to subsurface spalling in roller bearings. Liu et al. [21] examined the influences of horizontal and slant subsurface cracks on the contact characteristics of a roller bearing by using finite element method, and authors developed a mathematical relationship between the contact characteristics and the subsurface crack size using polynomial fitting. Elsharkawy [22] investigated the effect of friction on subsurface stresses in sliding line contact of multilayered elastic solids based on analytical method. Chidlow et al. [23] used analytical Fourier series solution for the local deflection and the subsurface stress field for the two-dimensional functionally graded elastic solid loaded by a pressure distribution. Savolainen and Lehtovaara [24] examined subsurface fatigue in rolling/sliding contact by experimentally based on a twin-disc test device and by computationally based on elastoplastic finite element model. Ali [25] conducted a computational study based on finite element analysis (FEA) to obtain subsurface stress in Hertzian contacts with sliding conditions. It was observed that sliding speed has a major effect on the value of maximum von-Mises stress in the subsurface of the contact. Arslan [26] developed a computational method to investigate frictional sliding contact problem between a laterally graded orthotropic medium and a rigid flat punch based on finite element analysis (FEA).

Research presented in the previous paragraph demonstrates the significance of subsurface stresses on fatigue and fracture behavior of elastic solids under contact conditions. However, these studies do not involve frictional heat generation. Heat generation on frictional contacts is an important phenomenon since it leads to thermal deformations on the contact surface. Liu et al. [27], Chen and Chen [28] respectively examined contact mechanics of FGM coating and contact mechanics of finite thickness FGM layer, both considering frictional heating. Steady state thermoelastic contact problem of FGM was studied by Barik et al. [29]. Choi and Paulino [30] analyzed the contact problem of homogenous coating/FGM interlayer and a substrate system involving frictional heat generation using analytical approach, and the effect of heat generation on contact stresses and punch stress intensity factors was examined. Thermoelastic properties of materials may change with temperature rise and the importance of the utilization of temperature dependent material properties was emphasized in wheel-rail sliding contact problems in [31-32]. Balci et al. [33] developed a computational method based on finite element analysis to find out the influence of temperature dependent properties on surface contact stresses in isotropic half-planes. Results showed that the utilization of temperature dependent material properties had a considerable effect on contact stresses. Balci et al. [34] further utilized the similar approach to examine the subsurface stresses in FGM coatings subjected to sliding contact with frictional heat generation. However, authors have not considered the variation of material properties due to the frictional heat generation. Hence, the influence of heat generation on subsurface stress distribution

within an elastic material under the effect of frictional contact has remained unknown yet.

The main novelty of this study is to find the effect of the use of temperature dependent material properties on subsurface stresses in an elastic solid subjected to thermoelastic contact. Hence, subsurface stresses are computed considering temperature independent and temperature dependent properties. Direct comparison between subsurface stress results shows that frictional heat leads to highest temperature change at close vicinity of the contact region and material properties mostly change at those locations, which results in higher levels of percent difference between subsurface stresses. Therefore, utilization of temperature dependent properties enables to better approximation to understand possible subsurface failures of elastic bodies under frictional contact with heat generation.

2. PROBLEM DESCRIPTION

The geometry of the addressed contact problem is depicted in Figure 1. The rigid punch has a flat profile and punch ends are denoted by a and b. (x, y) indicates the coordinate axes. Flat punch is located away from the coordinate axes and this distance is denoted by e. Punch slides over the medium at a slow velocity shown by V. P is the normal force vertically applied to the flat punch from its center. The tangential force Q is developed due to the friction on the contact surface and it is proportional to the normal force by a coefficient of friction η. q_f is the generated heat due to the frictional contact.

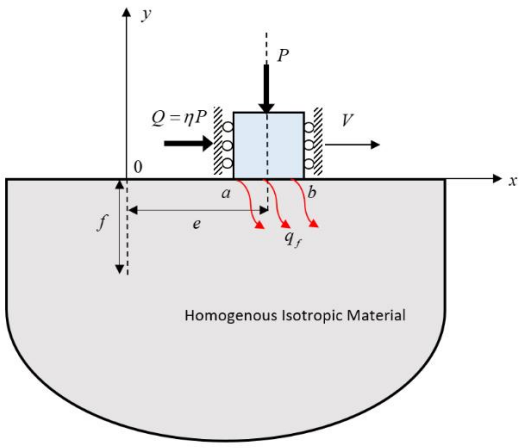

Figure 1. General schematic of the problem.

Contact problem is investigated utilizing general theory of thermoelasticity. Solution should be provided in both thermal and mechanical fields. First, thermal analysis is carried out and temperature distribution in the half-plane material is obtained. Obtained temperature field in the solid is applied to the half-plane while classical frictional contact mechanics analysis is being conducted. Then, contact stresses are obtained. The governing heat conduction equation in steady state reads:

$$k\nabla^2 T = 0, \tag{1}$$

where $\nabla^2 = \dfrac{\partial^2}{\partial x^2} + \dfrac{\partial^2}{\partial y^2}$. (2)

Inertia effects during sliding of the punch is neglected since convective effects would be much slower when compared to the effects of conduction. Hence, convective term in the heat equation, Eq. (1) is assumed zero. Note that all the heat flux due to friction flows towards the half-plane material. Related thermal boundary conditions are specified as follows [13]:

$$k\frac{dT(x,0)}{dy} = \begin{cases} -q_f(x) & a < x < b \\ 0 & x < a,\ x > b. \end{cases} \tag{3}$$

Surfaces out of the contact region are assumed thermally insulated which requires:

$$q_f(x) = 0, \quad -\infty < x < a,\ b < x < \infty. \tag{4}$$

Generated heat due to friction is calculated by the following formula [13, 30, 33-35]:

$$q_f(x) = V\,\sigma_{xy}(x,0), \quad a < x < b. \tag{5}$$

where V is the punch sliding velocity. The right and left far boundaries are thermally insulated. These boundary conditions are shown by,

$$q(-\infty, y) = 0, \quad -\infty < y < 0, \tag{6}$$

$$q(\infty, y) = 0, \quad -\infty < y < 0. \tag{7}$$

Temperature at far locations behind the contact is assumed to be the room temperature (300K) defined by T_0.

$$T(x, -\infty) = T_0\ , \quad -\infty < x < \infty. \tag{8}$$

It is considered that the surface of the half-plane material is an ideal surface without including any roughness. The constitutive relations for the two-dimensional elasticity problem can be expressed as two partial differential equations. These PDEs are produced by the substitution of elastic stress-strain relations into the equilibrium equation. This leads to the classical Navier equations of elasticity in a continuous medium [36]. The problem is dealt under small deformation theory and linear strain conditions. Navier equations are derived in the plane strain case as follows:

$$(\lambda+2\mu)\frac{\partial^2 u}{\partial x^2} + \mu\frac{\partial^2 u}{\partial y^2} + (\lambda+\mu)\frac{\partial^2 v}{\partial x \partial y} = \frac{\partial}{\partial x}\left((3\lambda+2\mu)\alpha T\right), \tag{9}$$

$$(\lambda+2\mu)\frac{\partial^2 v}{\partial y^2} + (\lambda+\mu)\frac{\partial^2 u}{\partial x \partial y} + \mu\frac{\partial^2 v}{\partial x^2} = \frac{\partial}{\partial y}\left((3\lambda+2\mu)\alpha T\right). \tag{10}$$

where λ is the Lame's constant and μ is the shear modulus.

$$\lambda = \frac{E\nu}{(1+\nu)(1-2\nu)}, \tag{11}$$

$$\mu = \frac{E}{2(1+\nu)}. \tag{12}$$

Stress-displacement relations can be expressed as:

$$\sigma_{xx}(x,y) = (\lambda + 2\mu)\frac{\partial u}{\partial x} + \lambda \frac{\partial v}{\partial y} - (3\lambda + 2\mu)\alpha T, \tag{13}$$

$$\sigma_{yy}(x,y) = \lambda\left(\frac{\partial u}{\partial x} + \frac{\partial v}{\partial y}\right) + 2\mu \frac{\partial v}{\partial y} - (3\lambda + 2\mu)\alpha T. \tag{14}$$

$$\sigma_{xy}(x,y) = \mu\left(\frac{\partial u}{\partial y} + \frac{\partial v}{\partial x}\right). \tag{15}$$

The following boundary conditions are applicable to the solution of the mechanical field. The normal and shear stress components out of the contact surface are zero.

$$\sigma_{yy}(x,0) = \sigma_{xy}(x,0) = 0, \quad -\infty < x < a, \quad b < x < \infty. \tag{16}$$

In the contact zone, the normal and shear stress are functions of lateral axis-*x* and they are expressed as:

$$\sigma_{yy}(x,0) = \sigma(x), \ \sigma_{xy}(x,0) = \eta\,\sigma(x), \quad a < x < b. \tag{17}$$

The vertical displacement component beneath the rigid punch is constant shown by v_0 because of the flat profile of the punch.

$$v(x,0) = v_0, \quad a < x < b, \tag{18}$$

$$\frac{\partial v(x,0)}{\partial y} = 0, \quad a < x < b. \tag{19}$$

The regularity conditions requires that all the displacement quantities should vanish at far points away from the contact. Hence,

$$u(x,\infty) = 0, \ v(x,\infty) = 0, \ -\infty < x < \infty. \tag{20}$$

The summation of the normal contact stress beneath the flat punch must be equal to the normal force applied to the rigid punch. This condition is named as equilibrium and it is indicated by,

$$\int_a^b \sigma_{yy}(x,0)\,dx = -P. \tag{21}$$

The following assumptions are made in the solution of the present thermoelastic contact problem as provided in [30].

- The punch is rigid and non-conductive therefore the flow of heat enters into the contacting material and other heat leakages are neglected.
- The free surface outside the contact area is thermally insulated.
- The motion of the punch is slow so that inertia effects are ignored.
- The contact area is stationary and there is no separation between the punch and the contact surface.

3. ALGORITHM AND THE FINITE ELEMENT PROCEDURE

An iterative computer code based on finite element analysis is developed. This iterative approach consists of sequential solutions for the thermal field and mechanical field. Generated heat on the contact surface depends on shear stress and the velocity of the punch. Heat flux is applied to the thermal model and temperature distribution is obtained. Then, obtained temperature distribution is applied as a body load to the mechanical field in which non-linear contact mechanics analysis takes place. Consecutive solutions of thermal and mechanical fields continue until generated heat on the contact surface arrives at equilibrium, Hence, strains due to the thermal expansion of the material is taken into account. Material properties are computed sequentially based on the temperature values in the elastic homogenous medium. The flowchart of this algorithm is originally developed by Balci et al. [33-34] and it is also depicted in Figure 2. This algorithm is implemented in ANSYS Parametric Design Language (APDL) [37] to obtain subsurface contact stresses.

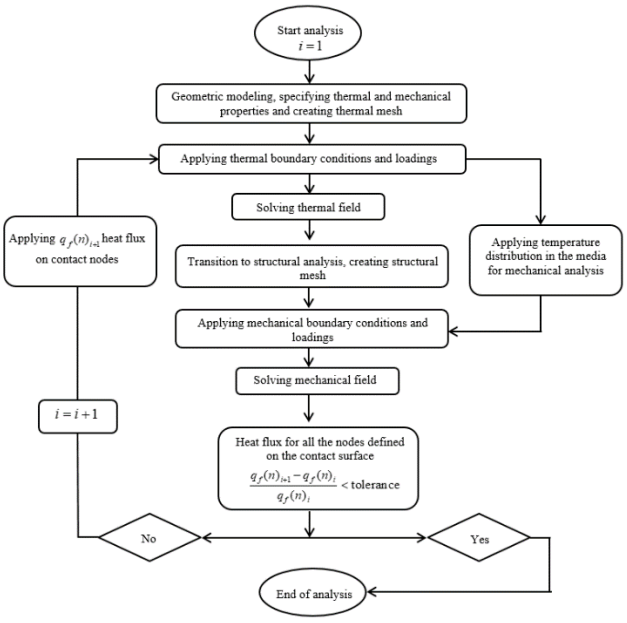

Figure 2. The flowchart of developed algorithm in ANSYS Mechanical APDL [37].

Constructed finite element mesh for the thermoelastic contact mechanics analysis is illustrated in Figure 3(a). L, H and pw respectively designated for model length, model height and punch width. In order to eliminate dimensional effects in two-dimensional finite element analysis, values of L and H are kept large with respect to punch width pw. Therefore, $\mathrm{pw}/L = 1/100$ and

$pw/H = 1/50$. Appearance of contact node discretization on the contact surface is shown in Figure 3(b).

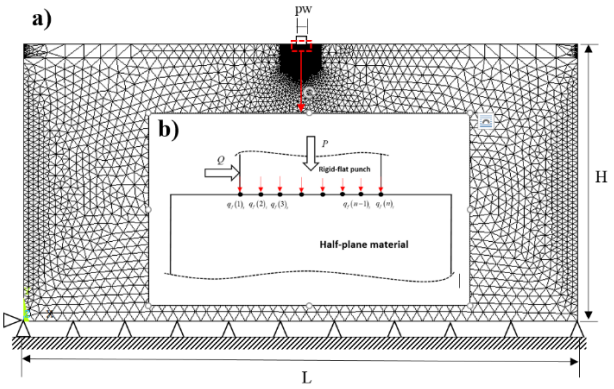

Figure 3. (a) Constructed finite element mesh for parametric analyses, (b) Contact surface discretization and schematic view presenting the applied heat flux $q_f(n)_i$ on the contact nodes.

Quadrilateral 8-node PLANE77 element and 8-node PLANE183 element types are utilized in thermal and mechanical analyses, respectively. In total 94622 8-node quadrilateral elements, 200 contact line elements named as CONTA172 and a target element called TARGE169 are used. Contact problem is solved computationally using the Augmented Lagrangian Method which is one of the well-known contact formulation schemes available in ANSYS Mechanical APDL [37].

4. NUMERICAL RESULTS

In this section, numerical results are obtained for the homogenous metallic half-plane (Ti-6Al-4V) under various thermomechanical conditions in plane strain case. Deformed mesh, temperature contours around the contact region and subsurface normal and lateral contact stresses are provided. Before proceeding with the parametric analyses, it is worth to define the dimensionless punch sliding velocity. Dimensionless punch sliding velocity is expressed in the study carried out by Choi and Paulino [30] as follows:

$$V_0 = \frac{\mu(1+\nu)\alpha\eta(b-a)/2}{4k(1-\nu)}V. \tag{22}$$

where μ is the shear modulus, ν is the Poisson's ratio, α is the thermal expansion coefficient, η is the coefficient of friction, k is the thermal conductivity, $(b-a)/2$ is the half-width of the flat punch and V is the nominal punch sliding velocity. When $V = 0.00$, problem transforms to the isothermal contact problem where there is no heat generation takes place. In other cases where $V \neq 0.00$, frictional heat is generated on the contact surface and this heat flows towards the metallic half-plane. The history of temperature variation can be taken into account by adding a convective term to the heat equation, Eq. (1). Nevertheless, such a convection term in the heat equation as well as the inertia terms in the Navier equations, Eqs. (9)-(10) are neglected since the effect of convection would be much smaller than that of conduction in case of slow sliding velocity of the punch [30]. Therefore, in the present study, convective effects during sliding are ignored. Subsurface stress is normalized utilizing the average contact stress defined as follows:

$$\sigma_0 = \frac{P}{(b-a)}. \tag{23}$$

Another normalization is required to express the coordinate axis y as a dimensionless coordinate parameter (Apatay et al. [38]):

$$y = \frac{b-a}{2}r + \frac{b+a}{2}, \quad -1 < r < 1. \tag{24}$$

4.1. Comparison and Validation of Results

Deformed mesh around the contact region is illustrated in Figure 4(a)-(b) for different values of punch sliding velocity. Coefficient of friction is set to $\eta = 0.3$ in both cases. In Figure 4(a), dimensionless punch sliding velocity is set to $V_0 = 0.00$ which corresponds to isothermal contact where no heat generation occurs, however in Figure 4(b), dimensionless punch sliding velocity is set to $V_0 = 0.10$ in which thermal effects are influential. It should be remarked that when punch sliding velocity is different from zero, frictional heat is generated on the contact surface and this heat leads to thermal expansion on the surface of the metallic half-plane. Since temperature levels are relatively high around the contact region, observed thermal expansion is greater there. This conclusion is drawn from comparing the deformed shape of metallic half-plane material indicated in Figure 4(a) and Figure 4(b). Figure 5 shows the temperature contours around the contact region for different values of coefficient of friction η while keeping the nominal sliding speed the same.

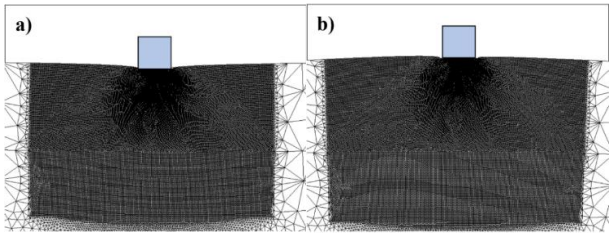

Figure 4. Deformed mesh around the contact region; a) $\eta = 0.3,\ V_0 = 0.00$, b) $\eta = 0.3, V_0 = 0.10$.

In order to observe the effect of coefficient of friction on heat generation and the temperature rising on the contact surface, nominal punch sliding velocity '*V*' is kept constant rather than dimensionless sliding velocity as in the study of Choi and Paulino [30]. Thus, at the same nominal sliding speed, the effect of coefficient of friction on temperature change can clearly be observed.

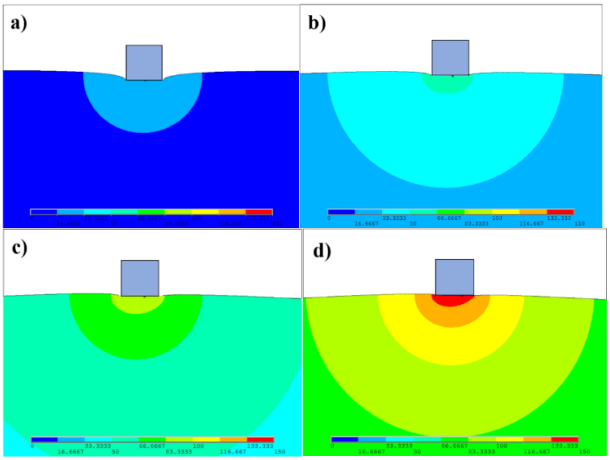

Figure 5. Contours of temperature change (ΔT) around the contact zone for different values of coefficient of friction $V = 74.3\,\mu m/s$. a) $\eta = 0.1$, b) $\eta = 0.3$, c) $\eta = 0.5$, d) $\eta = 0.8$.

Otherwise, if dimensionless sliding velocity was kept constant, it would cause a decrease in the nominal sliding velocity for higher values of coefficient of friction. Hence, a meaningful and slow nominal sliding velocity is chosen as $V = 74.3\,\mu m/s$ (Balci et al. [34]). This nominal sliding velocity corresponds to dimensionless velocities $V_0 = 0.02$, $V_0 = 0.06$, $V_0 = 0.10$ and $V_0 = 0.16$ for $\eta = 0.1$, $\eta = 0.3$, $\eta = 0.5$ and $\eta = 0.8$, respectively. Figure 6(a) and 6(b) respectively show the normal contact stress obtained by the present study and those obtained by Balci et al. [34] together. The former figure shows the normal contact stress distribution for different dimensionless punch velocities using temperature independent properties and the latter indicates normal contact stresses using temperature dependent properties. Contact stresses found by the present study are in a very good agreement with those presented in Balci et al. [34]. Apatay et al. [38] presented subsurface stresses in FGM

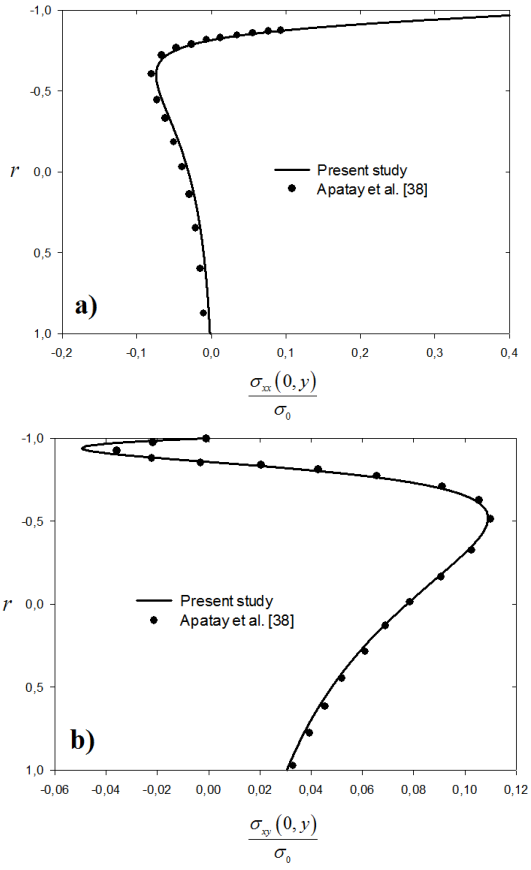

Figure 7. (a) Normal and (b) Shear subsurface stress distribution towards the thickness of the half-plane for isothermal contact $V_0 = 0.00$, $e/f = 0.25$, $a/e = 0.1$, $b/e = 0.4$, $\eta = 0.5$.

comparison study is performed comparing results of present study with those for homogenous case of the Apatay et al. [38]. Coefficient of friction is adjusted as $\eta = 0.5$, and same parametric values are utilized. Subsurface normal and shear contact stress distributions are depicted in Figure 7. Solid lines show the results of

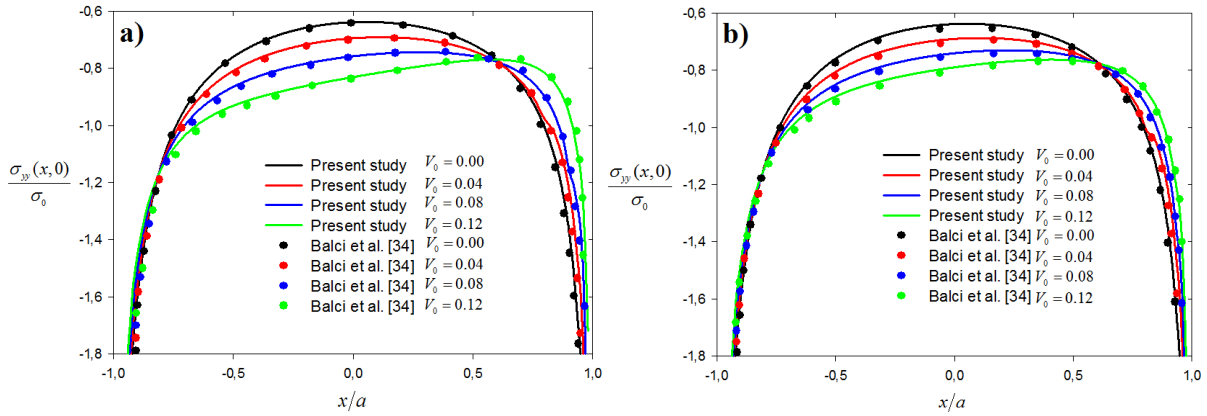

Figure 6. Normal contact stress distribution for half-plane contacts for various dimensionless punch sliding velocity, $\eta = 0.3$, (a) by the use of temperature independent properties, (b) by the use of temperature dependent properties.

coatings subjected to sliding contact without frictional heat generation using analytical method. Another

present study and dot points show those of Apatay et al. [38]. It can be seen in Figure 7 that results are highly

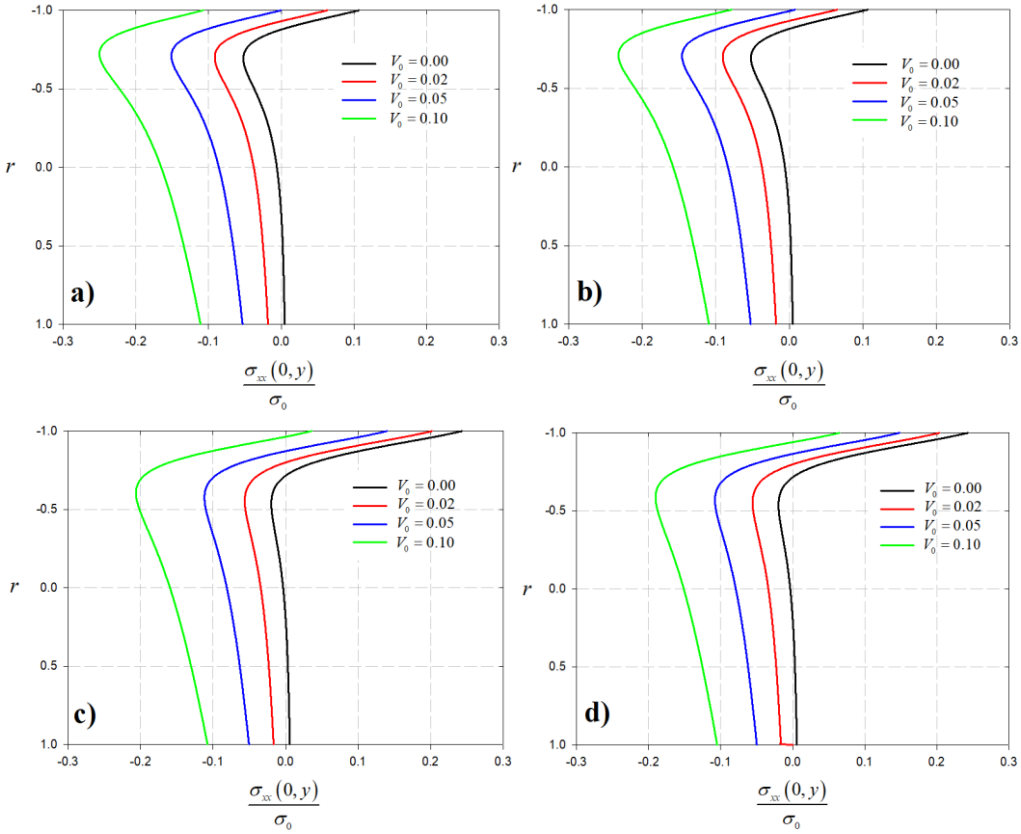

Figure 8. Subsurface normal stress towards thickness for various values of dimensionless sliding velocity $e/f = 2.0$, $a/e = 0.75$, $b/e = 1.25$; (a) $\eta = 0.3$ with temperature independent properties, (b) $\eta = 0.3$ with temperature dependent properties, (c) $\eta = 0.7$ with temperature independent properties, (d) $\eta = 0.7$ with temperature dependent properties.

compatible with each other. Therefore, another verification study is accomplished.

4.2. Subsurface Normal and Shear Stress Distributions

Subsurface normal and shear stress distributions are presented in this section. Figure 8(a)-(b) respectively show normal subsurface stresses utilizing temperature independent and temperature dependent properties by taking coefficient of friction $\eta = 0.3$. Figure 8(c)-(d) indicate those stresses by taking $\eta = 0.7$. As sliding velocity is increased, normal subsurface stresses tend to become much compressive towards the thickness of the half-plane. Moreover, when $\eta = 0.7$, the tensile behavior of normal subsurface stress is enhanced on the contact surface where $r = -1$, as depicted in Figure 8(c)-(d). Increase in dimensionless punch sliding velocity V_0 results in generation of greater frictional heat on the contact surface and this heat flows towards the half-plane material and changes material's termoelastic properties. Hence, greater heat generation leads to the occurrence of greater temperature change and therefore, material's thermoelastic properties vary much more. The impact of the utilization of temperature dependent material properties on subsurface stresses is profound especially at larger sliding speed $V_0 = 0.10$.

Figure 9(a)-(b) respectively indicate subsurface shear stresses using temperature independent and temperature dependent properties when $\eta = 0.3$. Figure 9(c)-(d) indicate those stresses when coefficient of friction is adjusted as $\eta = 0.7$. Increase in the coefficient of friction results in occurrence of greater compressive shear stresses in the interval $r \geq -1$, $r \leq -0.75$. However, subsurface shear stresses are less in the interval $r \leq -0.75$. $r \geq -0.50$ for $\eta = 0.7$. Increase in dimensionless punch sliding velocity does not significantly affect subsurface shear stresses in the interval of $r \geq -1$, $r \leq -0.5$. As sliding velocity is increased, subsurface shear stress tends to be slightly greater especially in the interval of $r \geq -0.5$, $r \leq 1.0$. Since obtained shear stresses are very close to each other, the influence of the utilization of temperature dependent properties need to be investigated quantitatively. Hence, tables are prepared to assess the influence of the utilization of temperature dependent properties on subsurface contact stresses.

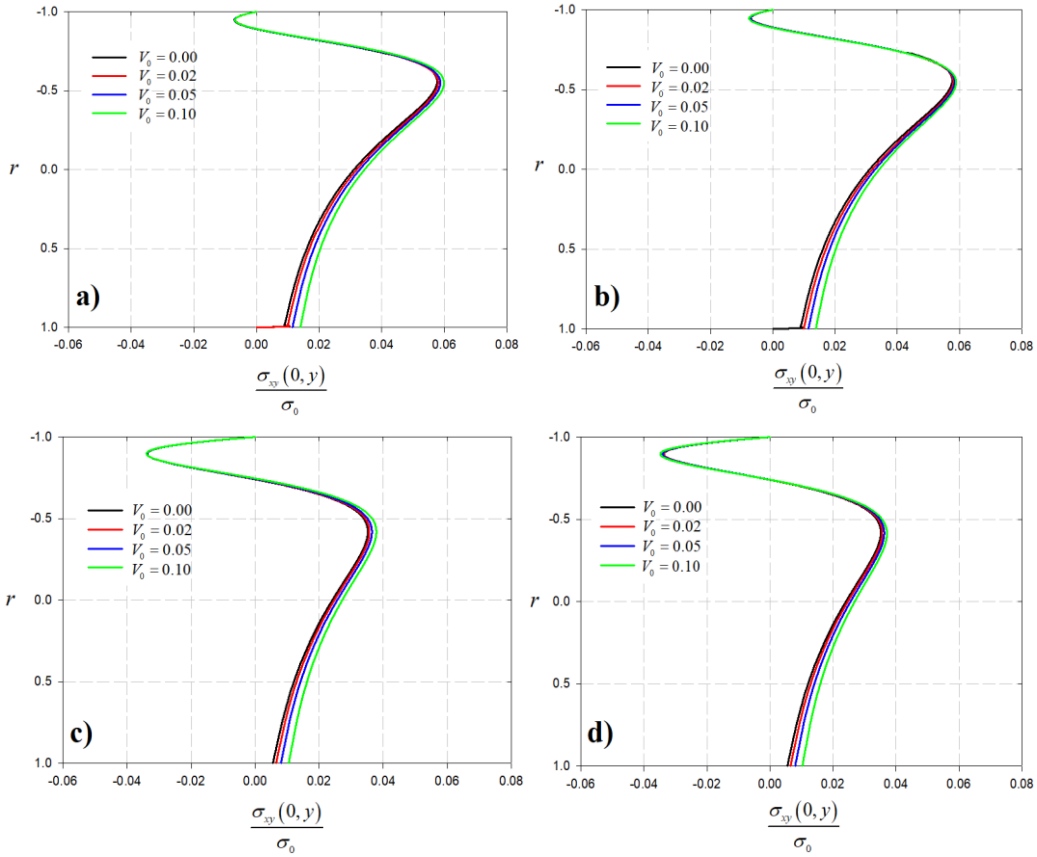

Figure 9. Subsurface shear stress towards thickness for various values of dimensionless sliding velocity $e/f = 2.0$; $a/e = 0.75$, $b/e = 1.25$; (a) $\eta = 0.3$ with temperature independent properties, (b) $\eta = 0.3$ with temperature dependent properties, (c) $\eta = 0.7$ with temperature independent properties, (d) $\eta = 0.7$ with temperature dependent properties.

In all tables, $(.)_C$ denotes the related normalized subsurface normal or shear stress value by the use of temperature independent properties and $(.)_D$ stands for those by the use of temperature dependent properties. Ti-6Al-4V is selected as a half-plane material and temperature dependent properties of this material are provided in Appendix-A (Ootao et al. [39]). $\varepsilon\%$ indicates the percent difference between subsurface stresses computed considering temperature independent and temperature dependent properties, and it is simply calculated by the following formula [34]:

$$\varepsilon\% = \left| \frac{(.)_D - (.)_C}{(.)_D} \right| \times 100. \tag{25}$$

Tables 1-2 show the comparison of normal and shear stresses when coefficient of friction is $\eta = 0.3$, and Tables 3-4 indicate this comparison study for $\eta = 0.7$. Table 1 shows subsurface normal contact stresses for different dimensionless sliding velocities at specified points towards the thickness of the half-plane. When Table 1 is examined, percent difference between subsurface normal contact stresses becomes larger at higher velocities of the punch, and level of this percent difference is observed greater at locations near the contact surface where $r \geq -1$ and $r \leq -0.6$. While percent differences vary between 0.8% - 8.14% for $V_0 = 0.02$, these values are in between 1.36% - 105.43% for punch speed $V_0 = 0.05$. When sliding velocity becomes $V_0 = 0.10$, percent difference values are 1.59% - 37.33%. Subsurface shear contact stresses and related percent difference values are tabulated in Table 2. As punch sliding velocity is increased, percent difference becomes greater for all values of r. Higher level of percent difference is observed near the contact surface and its maximum level is 17.57% at $r = -0.9$, for the velocity $V_0 = 0.02$. For punch velocities $V_0 = 0.05$ and $V_0 = 0.10$, the maximum of percent difference value is 17.20% and 41.22%, respectively. Table 3 presents the subsurface normal stress for different values of punch sliding velocity and percent difference between $(\sigma_{xx}(0,y)/\sigma_0)_C$ and $(\sigma_{xx}(0,y)/\sigma_0)_D$. At punch velocity $V_0 = 0.02$, difference values are observed between 0.75% and 98.92%. Moreover, at $V_0 = 0.10$, percent difference values are determined between 2.71% - 120.66%. This shows higher sliding velocity leads to a

Table 1. Subsurface normal stress distribution and percent difference for different dimensionless sliding velocity V_0; $\eta = 0.3,\ e/f = 2.0,\ a/e = 0.75,\ b/e = 1.25.$

	$V_0 = 0.02$			$V_0 = 0.05$			$V_0 = 0.10$		
r	$\left(\frac{\sigma_{xx}}{\sigma_0}\right)_C$	$\left(\frac{\sigma_{xx}}{\sigma_0}\right)_D$	$\varepsilon\%$	$\left(\frac{\sigma_{xx}}{\sigma_0}\right)_C$	$\left(\frac{\sigma_{xx}}{\sigma_0}\right)_D$	$\varepsilon\%$	$\left(\frac{\sigma_{xx}}{\sigma_0}\right)_C$	$\left(\frac{\sigma_{xx}}{\sigma_0}\right)_D$	$\varepsilon\%$
-1	0.0636	0.0661	**3.82**	-0.0005	0.0085	**105.43**	-0.1074	-0.0782	**37.33**
-0.96	0.0266	0.0290	**8.08**	-0.0368	-0.0284	**29.27**	-0.1427	-0.1153	**23.73**
-0.9	-0.0257	-0.0238	**8.14**	-0.0883	-0.0809	**9.20**	-0.1927	-0.1680	**14.67**
-0.8	-0.0788	-0.0775	**1.66**	-0.1401	-0.1339	**4.59**	-0.2417	-0.2211	**9.31**
-0.7	-0.0915	-0.0905	**1.01**	-0.1511	-0.1459	**3.53**	-0.2497	-0.2324	**7.43**
-0.6	-0.0853	-0.0845	**0.88**	-0.1431	-0.1387	**3.18**	-0.2386	-0.2239	**6.57**
-0.5	-0.0742	-0.0735	**0.89**	-0.1302	-0.1264	**3.04**	-0.2227	-0.2100	**6.05**
-0.4	-0.0635	-0.0629	**0.97**	-0.1178	-0.1144	**2.97**	-0.2075	-0.1964	**5.68**
-0.2	-0.0477	-0.0472	**1.12**	-0.0987	-0.0960	**2.83**	-0.1831	-0.1743	**5.03**
0	-0.0378	-0.0374	**1.23**	-0.0858	-0.0836	**2.64**	-0.1652	-0.1582	**4.41**
0.2	-0.0314	-0.0310	**1.27**	-0.0765	-0.0747	**2.41**	-0.1512	-0.1456	**3.81**
0.4	-0.0269	-0.0265	**1.27**	-0.0693	-0.0678	**2.16**	-0.1394	-0.1351	**3.23**
0.6	-0.0235	-0.0232	**1.23**	-0.0633	-0.0621	**1.90**	-0.1292	-0.1258	**2.67**
0.8	-0.0207	-0.0204	**1.17**	-0.0580	-0.0571	**1.63**	-0.1198	-0.1173	**2.13**
1	-0.0183	-0.0181	**1.10**	-0.0533	-0.0526	**1.36**	-0.1111	-0.1094	**1.59**

Table 2. Subsurface shear stress distribution and percent difference for different dimensionless sliding velocity V_0; $\eta = 0.3,\ e/f = 2.0,\ a/e = 0.75,\ b/e = 1.25.$

	$V_0 = 0.02$			$V_0 = 0.05$			$V_0 = 0.10$		
r	$\left(\frac{\sigma_{xy}}{\sigma_0}\right)_C$	$\left(\frac{\sigma_{xy}}{\sigma_0}\right)_D$	$\varepsilon\%$	$\left(\frac{\sigma_{xy}}{\sigma_0}\right)_C$	$\left(\frac{\sigma_{xy}}{\sigma_0}\right)_D$	$\varepsilon\%$	$\left(\frac{\sigma_{xy}}{\sigma_0}\right)_C$	$\left(\frac{\sigma_{xy}}{\sigma_0}\right)_D$	$\varepsilon\%$
-1	-1.131E-5	-1.134E-5	**0.23**	-1.131E-5	-1.140E-5	**0.75**	-1.135E-5	-1.158E-5	**1.96**
-0.96	-0.0065	-0.0067	**2.73**	-0.0066	-0.0068	**2.84**	-0.0066	-0.0071	**7.85**
-0.9	-0.0016	-0.0020	**17.57**	-0.0018	-0.0022	**17.20**	-0.0016	-0.0028	**41.22**
-0.8	0.0257	0.0254	**1.27**	0.0258	0.0253	**1.79**	0.0264	0.0249	**6.06**
-0.7	0.0481	0.0480	**0.33**	0.0485	0.0481	**0.83**	0.0495	0.0481	**2.93**
-0.6	0.0572	0.0572	**0.07**	0.0578	0.0575	**0.54**	0.0590	0.0579	**1.96**
-0.5	0.0573	0.0573	**0.03**	0.0580	0.0578	**0.40**	0.0592	0.0584	**1.47**
-0.4	0.0531	0.0532	**0.08**	0.0539	0.0537	**0.32**	0.0551	0.0545	**1.17**
-0.2	0.0418	0.0419	**0.10**	0.0427	0.0426	**0.24**	0.0441	0.0437	**0.87**
0	0.0320	0.0320	**0.09**	0.0330	0.0329	**0.23**	0.0345	0.0342	**0.77**
0.2	0.0246	0.0246	**0.07**	0.0257	0.0257	**0.24**	0.0275	0.0273	**0.79**
0.4	0.0190	0.0192	**0.80**	0.0204	0.0203	**0.28**	0.0224	0.0222	**0.88**
0.6	0.0151	0.0152	**0.74**	0.0166	0.0165	**0.34**	0.0187	0.0186	**0.99**
0.8	0.0122	0.0123	**0.66**	0.0137	0.0137	**0.41**	0.0161	0.0159	**1.13**
1	0.0100	0.0100	**0.04**	0.0115	0.0115	**0.50**	0.0141	0.0139	**1.30**

greater change in normal subsurface stresses for $\eta = 0.7$ again. Table 4 tabulates subsurface shear stresses towards thickness and percent difference is calculated between $\left(\sigma_{xy}(0,y)/\sigma_0\right)_C$ and $\left(\sigma_{xy}(0,y)/\sigma_0\right)_D$. While percent difference value $\varepsilon\%$ is in the interval of 0.01% - 0.94% for $V_0 = 0.02,$ this difference becomes 1.11% - 12.91% for $V_0 = 0.10.$ The maximum difference is observed at dimensionless coordinate $r = -0.7.$

The influence of coefficient of friction η on subsurface normal and shear stresses is illustrated in Figure 10. Normal and shear stresses are generated by keeping the nominal punch sliding velocity '*V*' the same instead of keeping 'V_0' in order to see the friction effect and its results on temperature distribution directly. As coefficient of friction η is increased, subsurface normal stress becomes significantly compressive throughout the thickness as depicted in Figure 10(a)-(b). When subsurface shear stresses are examined, it is clearly seen that increase in the coefficient of friction leads to greater tensile shear stresses between $r \geq -1,\ r \leq 0.$ Subsurface shear stresses gradually go to zero as dimensionless coordinate value r goes from -1 to 1.

Table 3. Subsurface normal stress distribution and percent difference for different dimensionless sliding velocity V_0; $\eta = 0.7,\ e/f = 2.0,\ a/e = 0.75,\ b/e = 1.25.$

	$V_0 = 0.02$			$V_0 = 0.05$			$V_0 = 0.10$		
r	$\left(\frac{\sigma_{xx}}{\sigma_0}\right)_C$	$\left(\frac{\sigma_{xx}}{\sigma_0}\right)_D$	$\varepsilon\%$	$\left(\frac{\sigma_{xx}}{\sigma_0}\right)_C$	$\left(\frac{\sigma_{xx}}{\sigma_0}\right)_D$	$\varepsilon\%$	$\left(\frac{\sigma_{xx}}{\sigma_0}\right)_C$	$\left(\frac{\sigma_{xx}}{\sigma_0}\right)_D$	$\varepsilon\%$
-1	0.2024	0.2039	**0.75**	0.1401	0.1483	**5.57**	0.0358	0.0651	**45.03**
-0.96	0.1607	0.1621	**0.88**	0.0989	0.1066	**7.27**	-0.0047	0.0229	**120.66**
-0.9	0.0909	0.0922	**1.38**	0.0298	0.0368	**19.03**	-0.0729	-0.0476	**53.22**
-0.8	0.0000	0.0011	**98.92**	-0.0598	-0.0539	**10.91**	-0.1604	-0.1388	**15.62**
-0.7	-0.0427	-0.0419	**2.02**	-0.1008	-0.0959	**5.15**	-0.1987	-0.1801	**10.30**
-0.6	-0.0554	-0.0547	**1.28**	-0.1117	-0.1075	**3.92**	-0.2064	-0.1904	**8.42**
-0.4	-0.0514	-0.0509	**1.01**	-0.1042	-0.1010	**3.19**	-0.1929	-0.1804	**6.92**
-0.5	-0.0555	-0.0549	**1.08**	-0.1100	-0.1064	**3.44**	-0.2016	-0.1876	**7.49**
-0.2	-0.0418	-0.0414	**0.97**	-0.0915	-0.0889	**2.89**	-0.1748	-0.1648	**6.12**
0	-0.0344	-0.0339	**1.55**	-0.0811	-0.0790	**2.63**	-0.1595	-0.1513	**5.47**
0.2	-0.0290	-0.0286	**1.44**	-0.0730	-0.0713	**2.38**	-0.1467	-0.1399	**4.87**
0.4	-0.0250	-0.0246	**1.31**	-0.0662	-0.0649	**2.12**	-0.1356	-0.1300	**4.30**
0.6	-0.0217	-0.0215	**1.18**	-0.0605	-0.0594	**1.86**	-0.1256	-0.1210	**3.76**
0.8	-0.0190	-0.0188	**1.09**	-0.0553	-0.0545	**1.59**	-0.1164	-0.1127	**3.23**
1	-0.0166	-0.0165	**0.53**	-0.0506	-0.0500	**1.33**	-0.1078	-0.1049	**2.71**

Table 4. Subsurface shear stress distribution and percent difference for different dimensionless sliding velocity V_0; $\eta = 0.7,\ e/f = 2.0,\ a/e = 0.75,\ b/e = 1.25.$

	$V_0 = 0.02$			$V_0 = 0.05$			$V_0 = 0.10$		
r	$\left(\frac{\sigma_{xy}}{\sigma_0}\right)_C$	$\left(\frac{\sigma_{xy}}{\sigma_0}\right)_D$	$\varepsilon\%$	$\left(\frac{\sigma_{xy}}{\sigma_0}\right)_C$	$\left(\frac{\sigma_{xy}}{\sigma_0}\right)_D$	$\varepsilon\%$	$\left(\frac{\sigma_{xy}}{\sigma_0}\right)_C$	$\left(\frac{\sigma_{xy}}{\sigma_0}\right)_D$	$\varepsilon\%$
-1	-1.191E-5	-1.192E-5	**0.10**	-1.20E-5	-1.20E-5	**0.48**	-1.21E-5	-1.23E-5	**1.32**
-0.96	-0.0214	-0.0215	**0.18**	-0.0215	-0.0217	**0.71**	-0.0217	-0.0221	**1.95**
-0.9	-0.0337	-0.0338	**0.24**	-0.0338	-0.0341	**0.93**	-0.0339	-0.0348	**2.64**
-0.8	-0.0164	-0.0165	**0.65**	-0.0161	-0.0166	**2.63**	-0.0156	-0.0170	**7.96**
-0.7	0.0104	0.0103	**0.94**	0.0109	0.0105	**3.98**	0.0120	0.0106	**12.91**
-0.6	0.0273	0.0272	**0.27**	0.0280	0.0276	**1.23**	0.0293	0.0282	**4.14**
-0.5	0.0344	0.0344	**0.15**	0.0352	0.0349	**0.73**	0.0366	0.0357	**2.56**
-0.4	0.0356	0.0356	**0.10**	0.0364	0.0362	**0.52**	0.0378	0.0371	**1.87**
-0.2	0.0311	0.0311	**0.05**	0.0319	0.0318	**0.33**	0.0333	0.0329	**1.29**
0	0.0247	0.0247	**0.03**	0.0256	0.0256	**0.27**	0.0272	0.0269	**1.11**
0.2	0.0192	0.0192	**0.02**	0.0202	0.0202	**0.27**	0.0220	0.0217	**1.11**
0.4	0.0147	0.0147	**0.01**	0.0159	0.0159	**0.30**	0.0178	0.0176	**1.24**
0.6	0.0113	0.0113	**0.02**	0.0126	0.0126	**0.36**	0.0148	0.0146	**1.45**
0.8	0.0087	0.0087	**0.03**	0.0101	0.0101	**0.44**	0.0124	0.0122	**1.71**
1	0.0065	0.0065	**0.04**	0.0080	0.0080	**0.57**	0.0105	0.0103	**2.05**

The utilization of temperature dependent properties is more profound for surfaces possessing greater coefficient of friction. Difference between stresses considering temperature independent and temperature dependent properties can clearly be seen in Figure 10(a)-(b) at $\eta = 0.8.$ However, this difference could not be clearly seen for subsurface shear stresses. Therefore, we present tables to find out the influence of the utilization of temperature dependent properties upon subsurface stresses, quantitatively.

Tables 5-6 show subsurface normal and shear stresses for different values of coefficient of friction η at specified dimensionless coordinate towards the thickness. Percent difference value is calculated as well. Subsurface normal stresses and related percent difference values between $\left(\sigma_{xx}(0,y)/\sigma_0\right)_C$ and $\left(\sigma_{xx}(0,y)/\sigma_0\right)_D$ are presented in Table 5. It can obviously be seen in Table 5 that percent difference value is gradually increasing for greater values of coefficient of friction. Percent difference value takes its maximum level around the contact surface where $r \geq -1,$ and $r \leq -0.8$ due to the occurrence of greatest temperature change around the contact. While going away from the contact surface, temperature change diminishes which causes a gradual decrease in percent

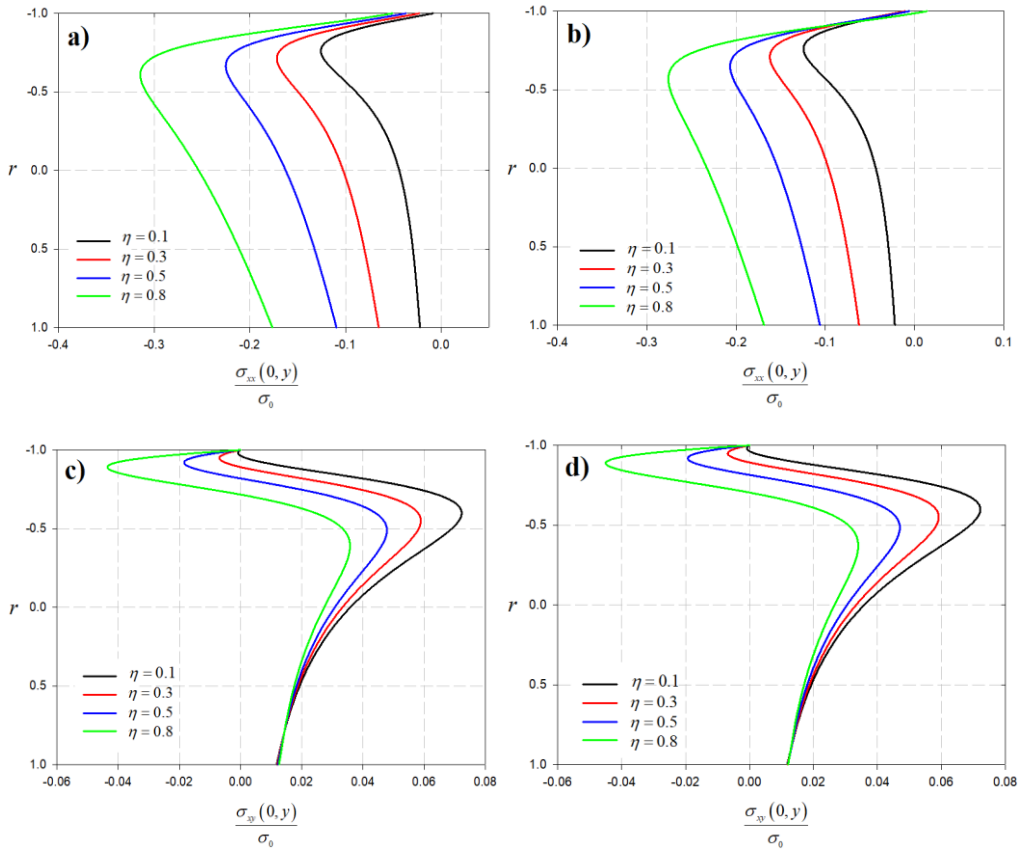

Figure 10. Subsurface normal and shear stress distributions towards thickness for various values of coefficient of friction $V = 74.3\,\mu m/s$, $e/f = 2.0$, $a/e = 0.75$, $b/e = 1.25$; (a) σ_{xx}/σ_0 utilizing temperature independent properties, (b) σ_{xx}/σ_0 utilizing temperature dependent properties, (c) σ_{xy}/σ_0 utilizing temperature independent properties, (d) σ_{xy}/σ_0 utilizing temperature dependent properties.

difference values towards the thickness. $\varepsilon\%$ varies between 4.97%-121.12% for $\eta = 0.3$, 3.28% - 548.10% for $\eta = 0.5$ and 4.52% - 460.28% for $\eta = 0.8$. When percent difference values are investigated in Table 5, the importance of the utilization of temperature dependent material properties is apperceived. Table 6 shows subsurface shear stresses and related percent difference values. Levels of percent difference are greater between dimensionless coordinate $r \geq -0.9$ and $r \leq -0.6$. Percent difference value becomes critical levels such as 285.6% for $\eta = 0.8$ at $r = -0.7$.

Subsurface normal and shear stresses are obtained for different values of $e/(b-a)$ ratio. When $e/(b-a) < 0$, it means that the path on which subsurface stresses are calculated is behind the punch, and $e/(b-a) > 0$ means that the path lies in front of the punch. While approaching the flat punch through its trailing end, normal contact stress tends to become much compressive in the region $r \leq -0.5$ and $r > -1$ as expected. In a similar fashion, while approaching the flat punch through its leading end, normal contact stress tends to be much compressive again. However, the severity of normal stress is larger behind the flat punch as shown in Figure 11(a)-(b). Moreover, subsurface shear stress distributions are obtained and they are plotted in Figure 11(c)-(d). Shear stress behind the trailing end of the punch is compressive for $e/(b-a) = -4$, $e/(b-a) = -2$ and $e/(b-a) = -1$. However, shear stress in front of the punch for $e/(b-a) = 1$, $e/(b-a) = 2$ and $e/(b-a) = 4$ can reach tensile levels. Subsurface stresses and related percent difference values are computed with respect to various values of dimensionless coordinate r and they are presented in Table 7-8.

Table 7 shows subsurface normal stresses and percent differences. In the region $r \geq -1$ and $r \leq -0.8$, percent difference decreases as the ratio $e/(b-a)$ goes from -4 to -1. However, in $r \geq -0.7$ and $r \leq 1$, percent differences slightly increase. Percent difference values observed in front of the flat punch at $e/(b-a) = 2$ are greater than those observed behind the punch and they can reach almost 120.66% at $r = -0.96$. Table 8 indicates subsurface shear stresses and related percent differences for various $e/(b-a)$ ratio. The level of percent

Table 5. Subsurface normal contact stress distribution and percent difference for different coefficient of friction η; $V = 74.3\,\mu\text{m/s},\ e/f = 2.0,\ a/e = 0.75,\ b/e = 1.25.$

	$\eta = 0.3$			$\eta = 0.5$			$\eta = 0.8$		
r	$\left(\frac{\sigma_{xx}}{\sigma_0}\right)_C$	$\left(\frac{\sigma_{xx}}{\sigma_0}\right)_D$	$\varepsilon\%$	$\left(\frac{\sigma_{xx}}{\sigma_0}\right)_C$	$\left(\frac{\sigma_{xx}}{\sigma_0}\right)_D$	$\varepsilon\%$	$\left(\frac{\sigma_{xx}}{\sigma_0}\right)_C$	$\left(\frac{\sigma_{xx}}{\sigma_0}\right)_D$	$\varepsilon\%$
-1	-0.0227	-0.0103	**121.17**	-0.0368	-0.0057	**548.10**	-0.0509	0.0141	**460.28**
-0.96	-0.0588	-0.0470	**24.99**	-0.0746	-0.0453	**64.81**	-0.0929	-0.0308	**202.16**
-0.9	-0.1100	-0.0990	**11.07**	-0.1334	-0.1067	**25.05**	-0.1664	-0.1082	**53.86**
-0.8	-0.1612	-0.1511	**6.67**	-0.2012	-0.1784	**12.78**	-0.2634	-0.2118	**24.37**
-0.7	-0.1716	-0.1622	**5.79**	-0.2241	-0.2045	**9.58**	-0.3062	-0.2612	**17.20**
-0.6	-0.1629	-0.1542	**5.67**	-0.2224	-0.2054	**8.31**	-0.3145	-0.2754	**14.20**
-0.5	-0.1495	-0.1413	**5.78**	-0.2121	-0.1970	**7.65**	-0.3084	-0.2739	**12.56**
-0.4	-0.1365	-0.1289	**5.92**	-0.2002	-0.1867	**7.23**	-0.2975	-0.2668	**11.48**
-0.2	-0.1163	-0.1096	**6.10**	-0.1790	-0.1680	**6.58**	-0.2742	-0.2493	**10.01**
0	-0.1023	-0.0965	**6.10**	-0.1624	-0.1533	**5.99**	-0.2534	-0.2328	**8.88**
0.2	-0.0921	-0.0869	**5.96**	-0.1490	-0.1414	**5.41**	-0.2352	-0.2180	**7.89**
0.4	-0.0839	-0.0793	**5.76**	-0.1376	-0.1312	**4.86**	-0.2188	-0.2045	**6.98**
0.6	-0.0770	-0.0730	**5.52**	-0.1274	-0.1222	**4.32**	-0.2038	-0.1920	**6.13**
0.8	-0.0709	-0.0673	**5.25**	-0.1182	-0.1138	**3.80**	-0.1897	-0.1801	**5.31**
1	-0.0653	-0.0622	**4.97**	-0.1095	-0.1060	**3.28**	-0.1764	-0.1688	**4.52**

Table 6. Subsurface shear contact stress distribution and percent difference for different coefficient of friction η; $V = 74.3\,\mu\text{m/s},\ e/f = 2.0,\ a/e = 0.75,\ b/e = 1.25.$

	$\eta = 0.3$			$\eta = 0.5$			$\eta = 0.8$		
r	$\left(\frac{\sigma_{xy}}{\sigma_0}\right)_C$	$\left(\frac{\sigma_{xy}}{\sigma_0}\right)_D$	$\varepsilon\%$	$\left(\frac{\sigma_{xy}}{\sigma_0}\right)_C$	$\left(\frac{\sigma_{xy}}{\sigma_0}\right)_D$	$\varepsilon\%$	$\left(\frac{\sigma_{xy}}{\sigma_0}\right)_C$	$\left(\frac{\sigma_{xy}}{\sigma_0}\right)_D$	$\varepsilon\%$
-1	-1.130E-5	-1.140E-5	**0.82**	-1.172E-5	-1.194E-5	**1.77**	-1.287E-5	-1.294E-5	**0.56**
-0.96	-0.0066	-0.0065	**1.67**	-0.0140	-0.0145	**3.52**	-0.0265	-0.0269	**1.80**
-0.9	-0.0018	-0.0015	**19.12**	-0.0174	-0.0185	**5.56**	-0.0433	-0.0446	**3.04**
-0.8	0.0258	0.0263	**1.58**	0.0056	0.0043	**32.20**	-0.0258	-0.0286	**9.87**
-0.7	0.0487	0.0491	**0.77**	0.0308	0.0295	**4.44**	0.0046	0.0012	**285.6**
-0.6	0.0580	0.0583	**0.51**	0.0441	0.0430	**2.53**	0.0244	0.0214	**14.38**
-0.5	0.0582	0.0585	**0.39**	0.0478	0.0470	**1.81**	0.0334	0.0309	**7.99**
-0.4	0.0542	0.0543	**0.31**	0.0464	0.0457	**1.44**	0.0358	0.0339	**5.59**
-0.2	0.0430	0.0431	**0.19**	0.0386	0.0382	**1.10**	0.0327	0.0315	**3.56**
0	0.0333	0.0333	**0.08**	0.0308	0.0305	**1.03**	0.0273	0.0266	**2.84**
0.2	0.0261	0.0261	**0.05**	0.0247	0.0244	**1.10**	0.0227	0.0221	**2.69**
0.4	0.0208	0.0208	**0.20**	0.0201	0.0198	**1.28**	0.0190	0.0185	**2.87**
0.6	0.0170	0.0170	**0.36**	0.0167	0.0165	**1.51**	0.0163	0.0158	**3.25**
0.8	0.0142	0.0142	**0.54**	0.0143	0.0140	**1.79**	0.0143	0.0138	**3.71**
1	0.0121	0.0120	**0.74**	0.0123	0.0120	**2.11**	0.0126	0.0121	**4.29**

difference for subsurface shear stress seems small when compared to that observed in Table 7. It can be inferred from Table 8 that obtained percent difference values are greater in front of the flat punch for most of the dimensionless coordinate value r.

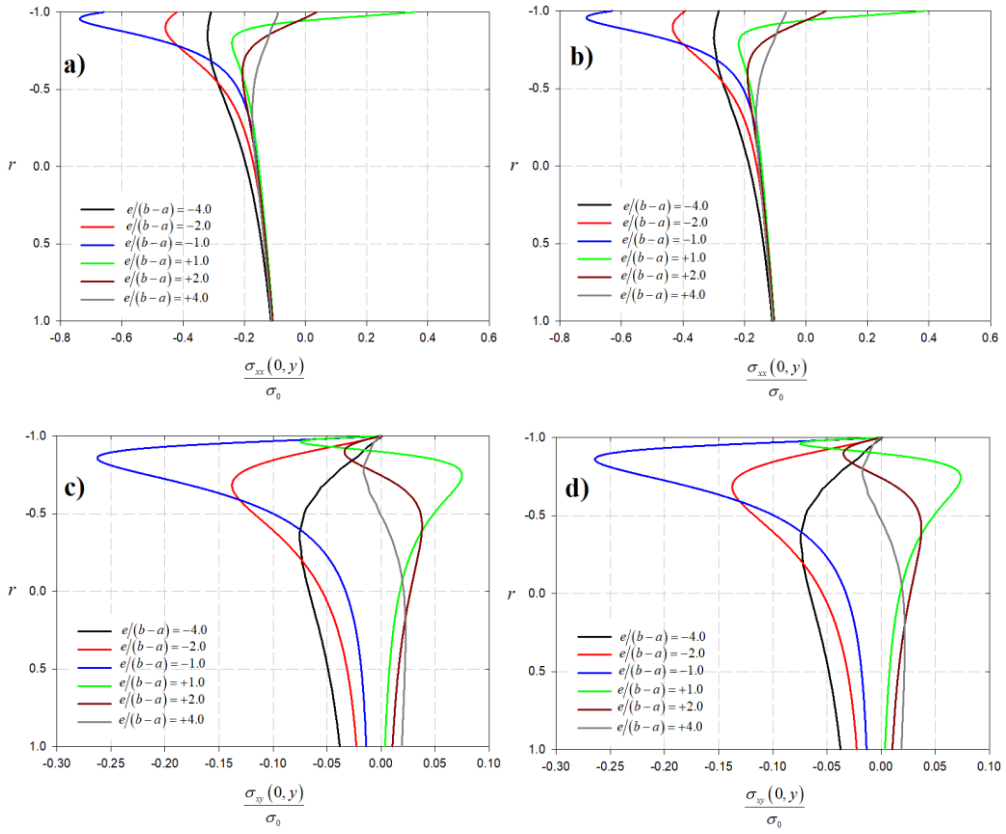

Figure 11. Subsurface normal and shear contact stress distributions towards thickness for various $e/(b-a)$ ratio $\eta = 0.7$, $V_0 = 0.10$, $(b-a)/f = 0.1$. (a) σ_{xx}/σ_0 utilizing temperature independent properties, (b) σ_{xx}/σ_0 utilizing temperature dependent properties, (c) σ_{xy}/σ_0 utilizing temperature independent properties, (d) σ_{xy}/σ_0 utilizing temperature dependent properties.

Table 7. Subsurface normal contact stress distribution and percent difference for different $e/(b-a)$ ratio $\eta = 0.7$, $V_0 = 0.10$.

	$e/(b-a) = -4$			$e/(b-a) = -1$			$e/(b-a) = 2$		
r	$\left(\frac{\sigma_{xx}}{\sigma_0}\right)_C$	$\left(\frac{\sigma_{xx}}{\sigma_0}\right)_D$	$\varepsilon\%$	$\left(\frac{\sigma_{xx}}{\sigma_0}\right)_C$	$\left(\frac{\sigma_{xx}}{\sigma_0}\right)_D$	$\varepsilon\%$	$\left(\frac{\sigma_{xx}}{\sigma_0}\right)_C$	$\left(\frac{\sigma_{xx}}{\sigma_0}\right)_D$	$\varepsilon\%$
-1	-0.3093	-0.2839	**8.93**	-0.6583	-0.6295	**4.57**	0.0358	0.0651	**45.03**
-0.96	-0.3136	-0.2894	**8.37**	-0.7374	-0.7138	**3.30**	-0.0047	0.0229	**120.66**
-0.9	-0.3185	-0.2959	**7.66**	-0.6526	-0.6285	**3.83**	-0.0729	-0.0476	**53.22**
-0.8	-0.3190	-0.2989	**6.74**	-0.4459	-0.4234	**5.31**	-0.1604	-0.1388	**15.62**
-0.7	-0.3093	-0.2913	**6.19**	-0.3221	-0.3031	**6.28**	-0.1987	-0.1801	**10.30**
-0.6	-0.2969	-0.2807	**5.76**	-0.2562	-0.2399	**6.80**	-0.2064	-0.1904	**8.42**
-0.5	-0.2787	-0.2643	**5.46**	-0.2196	-0.2054	**6.94**	-0.2016	-0.1876	**7.49**
-0.4	-0.2596	-0.2466	**5.25**	-0.1974	-0.1847	**6.85**	-0.1929	-0.1804	**6.92**
-0.2	-0.2232	-0.2126	**4.96**	-0.1715	-0.1613	**6.34**	-0.1748	-0.1648	**6.12**
0	-0.1934	-0.1848	**4.65**	-0.1554	-0.1470	**5.70**	-0.1595	-0.1513	**5.47**
0.2	-0.1701	-0.1630	**4.32**	-0.1431	-0.1363	**5.06**	-0.1467	-0.1399	**4.87**
0.4	-0.1518	-0.1460	**3.95**	-0.1327	-0.1270	**4.45**	-0.1356	-0.1300	**4.30**
0.6	-0.1368	-0.1322	**3.53**	-0.1232	-0.1186	**3.87**	-0.1256	-0.1210	**3.76**
0.8	-0.1243	-0.1206	**3.10**	-0.1144	-0.1107	**3.32**	-0.1164	-0.1127	**3.23**
1	-0.1133	-0.1104	**2.64**	-0.1061	-0.1032	**2.78**	-0.1078	-0.1049	**2.71**

Table 8. Subsurface shear contact stress distribution and percent difference for different $e/(b-a)$ ratio $\eta = 0.7, V_0 = 0.10$.

	$e/(b-a) = -4$			$e/(b-a) = -1$			$e/(b-a) = 2$		
r	$\left(\frac{\sigma_{xy}}{\sigma_0}\right)_C$	$\left(\frac{\sigma_{xy}}{\sigma_0}\right)_D$	$\varepsilon\%$	$\left(\frac{\sigma_{xy}}{\sigma_0}\right)_C$	$\left(\frac{\sigma_{xy}}{\sigma_0}\right)_D$	$\varepsilon\%$	$\left(\frac{\sigma_{xy}}{\sigma_0}\right)_C$	$\left(\frac{\sigma_{xy}}{\sigma_0}\right)_D$	$\varepsilon\%$
-1	7.683E-4	7.947E-4	**3.32**	1.185E-4	1.257E-4	**5.78**	-1.213E-5	-1.230E-5	**1.32**
-0.96	-0.0068	-0.0065	**4.12**	-0.1250	-0.1278	**2.19**	-0.0217	-0.0221	**1.95**
-0.9	-0.0168	-0.0162	**3.78**	-0.2455	-0.2489	**1.35**	-0.0339	-0.0348	**2.64**
-0.8	-0.0352	-0.0342	**2.79**	-0.2447	-0.2446	**0.02**	-0.0156	-0.0170	**7.96**
-0.7	-0.0507	-0.0496	**2.23**	-0.1862	-0.1851	**0.57**	0.0120	0.0106	**12.91**
-0.6	-0.0623	-0.0611	**1.93**	-0.1355	-0.1345	**0.79**	0.0293	0.0282	**4.14**
-0.5	-0.0711	-0.0700	**1.63**	-0.0998	-0.0989	**0.90**	0.0366	0.0357	**2.56**
-0.4	-0.0746	-0.0735	**1.54**	-0.0755	-0.0747	**0.97**	0.0378	0.0371	**1.87**
-0.2	-0.0732	-0.0722	**1.41**	-0.0472	-0.0467	**1.06**	0.0333	0.0329	**1.29**
0	-0.0666	-0.0657	**1.39**	-0.0327	-0.0323	**1.16**	0.0272	0.0269	**1.11**
0.2	-0.0590	-0.0582	**1.43**	-0.0247	-0.0244	**1.25**	0.0220	0.0217	**1.11**
0.4	-0.0520	-0.0513	**1.51**	-0.0200	-0.0197	**1.34**	0.0178	0.0176	**1.24**
0.6	-0.0462	-0.0455	**1.60**	-0.0170	-0.0168	**1.41**	0.0148	0.0146	**1.45**
0.8	-0.0418	-0.0411	**1.69**	-0.0151	-0.0149	**1.48**	0.0124	0.0122	**1.71**
1	-0.0382	-0.0375	**1.79**	-0.0137	-0.0135	**1.53**	0.0105	0.0103	**2.05**

5. CONCLUSIONS

Frictional contact mechanics between a homogenous elastic half-plane and a rigid flat punch is carried out using computational technique. Friction and the punch velocity on the contact surface leads to heat generation and this heat directly flows towards the half-plane material (Ti-6Al-4V). The variation in material's thermoelastic properties due to the change in temperature is considered in the present study. In order to obtain subsurface stresses, solution algorithm is developed, and it is implemented in ANSYS Parametric Design Language (APDL) [37]. Solution of the contact problem is attained by adopting an iterative scheme which requires consecutive analyses to the contact problem until generated heat on the contact surface reaches equilibrium. Determination of subsurface stresses are highly critical to assess the durability, wear and fatigue life of machine components. Following conclusions can be drawn from this study:

- Increase in the punch velocity leads to the occurrence of greater compressive normal stresses through the thickness. This compressive behavior in normal stress weakens at far locations in the medium. Tensile behavior in normal stress is enhanced on the contact surface ($r = -1$) due to the increase in the coefficient of friction at the same dimensionless speed (V_0).
- Shear stress is compressive just below the contact region, it gradually increases and becomes tensile level inside the medium. The strength of this compressive stress is obvious around the contact region.
- The change in the shear stress due to punch velocity is relatively lower when compared to that observed in the normal stress. As a result, normal subsurface stress is said to be more sensitive to the change in the punch velocity.
- As coefficient of friction is increased, the strength of the compressive normal stress increases towards the depth. Increase in the coefficient of friction results in a formation of greater compressive shear stress near the contact region.
- Subsurface stresses are examined at different paths consisting of behind and front sites of the punch. Normal and shear stresses are observed compressive behind the punch and they tend to be tensile in front of the punch. While going far away from contact region $|e/(b-a)| \to \infty$, the magnitude of these stresses gradually decreases.
- Higher level of punch speed and coefficient of friction results in a generation of greater frictional heat on the contact surface. Temperature reaches maximum levels at while coming close to contact surface. The influence of the utilization of temperature dependent material properties on subsurface stresses is remarkable and this effect is examined in tables. As normalized punch velocity is increased, the percent difference between subsurface stresses calculated based on temperature independent and temperature dependent properties increases. The maximum percent difference between normal stresses is observed just below the contact surface $-1 \le r \le -0.9$ while the maximum difference between subsurface shear stresses is seen around $r \ge -0.9$.
- The most of percent difference levels between subsurface stresses calculated based on temperature independent and temperature dependent properties are greater at locations close to contact surface and ahead of the leading end of the punch.

In order to design machine components subjected to frictional contact involving heat generation, subsurface contact stresses should be calculated considering temperature dependent material properties. Hence, results of this study may provide a better approximation to understand wear and fatigue behavior of materials subjected to frictional contacts with heat generation.

APPENDIX-A

Temperature dependent material properties for Ti-6Al-4V (Ootao et al. [39]):

$$E(T) = 122.7 - 0.0565\,T \quad \text{GPa}, \tag{A.1}$$

$$\alpha(T) = \begin{cases} 7.43\times10^{-6} + 5.56\times10^{-9}\,T - 2.69\times10^{-12}\,T^2\,(1/K), & 300K \le T \le 1100K, \\ 10.291\times10^{-6}\ \ (1/K), & 1100K \le T \le 1300K. \end{cases} \tag{A.2}$$

$$k(T) = 1.1 + 0.017\,T \quad (W/mK), \tag{A.3}$$

$$\nu(T) = 0.2888 + 32\times10^{-6}\,T. \tag{A.4}$$

ACKNOWLEDGEMENTS

Author presents his sincere thanks to the Editor and the Reviewers of the Journal of Polytechnic (Politeknik Dergisi) for thier valuable revision process which provides significant improvement on the present study.

DECLARATION OF ETHICAL STANDARDS

The author(s) of this article declare that the materials and methods used in this study do not require ethical committee permission and/or legal-special permission.

AUTHORS' CONTRIBUTIONS

Mehmet Nurullah BALCİ: Proposed the research topic and developed the computational method in the solution of the problem. Generated parametric results and compared them with those available in the literature. Arranged the general structure of the study and wrote the manuscript.

CONFLICT OF INTEREST

There is no conflict of interest in this study.

REFERENCES

[1] Hertz H., "On the contact of elastic solids", ***Journal für die Reine und Angewandte Mathematik***, 92: 156-171, (1881).

[2] Johnson K.L., "Contact mechanics", Cambridge: ***Cambridge University Press***, UK, (1985).

[3] Jaeger J. C., "Moving sources of heat and the temperature of sliding contacts", ***Proceedings of The Royal Society of NSW***, 76: 203–24 Part III, (1942).

[4] Barber J.R., "Some thermoelastic contact problems involving frictional heating", ***Journal of Applied Mathematics and Mechanics***, XXIX(1): 1–13, (1976).

[5] Dundurs J. and Comninou M., "Green's functions for planar thermoelastic contact problems – exterior contact", ***Mechanics Research Communications***, 6(5): 309–16, (1979).

[6] Comninou M. and Dundurs J., "On lack of uniqueness in heat conduction through a solid to solid contact", ***Journal of Heat Transfer***, 102: 319-323, (1980).

[7] Comninou M., Dundurs J., Barber J.R., "Planar Hertz contact with heat conduction", ***Journal of Applied Mechanics***, 48: 549-554, (1981).

[8] Comninou M., Barber, J.R., Dundurs, J., "Heat conduction through a flat punch", ***Journal of Applied Mechanics***, 48:871-875, (1981).

[9] Dundurs J. and Comninou M., "Green's function for planar thermoelastic contact problems - -interior contact", ***Mechanics Research Communications***, 6: 317-321, (1979).

[10] Barber, J.R. and Martin-Moran, C.J., "Green's functions for transient thermoelastic contact problems for the half-plane", ***Wear***, 79: 11-19, (1982).

[11] Hills, D.A. and Barber J.R., "Steady motion of an insulating rigid flat –ended punch over a thermally conducting half-plane", ***Wear***, 102: 15-22, (1985).

[12] Kulchytsky-Zhyhailo R.D. and Yevtushenko A.A., "Approximate method for analysis of the contact temperature and pressure due to frictional load in an elastic layered medium", ***International Journal of Solids and Structures***, 35: 319-329, (1998).

[13] Chao C.-K. and Gao B., "Rigid stamp indentation for a thermoelastic half-plane", ***International Journal of Solids and Structures***, 37: 4635-4654, (2000).

[14] Matysiak J. and Yevtushenko A.A., "On heating problems of friction", ***Journal of Theoretical and Applied Mechanics***, 3:39, (2001).

[15] Guler M.A. and Erdogan F., "Contact mechanics of graded coatings", ***International Journal of Solids and Structures***, 41: 3865-3889, (2004).

[16] Guler M.A. and Erdogan F., "The frictional sliding contact problems of rigid parabolic and cylindrical stamps on graded coatings", ***International Journal of Mechanical Sciences***, 49: 161-182, (2007).

[17] Dag S. and Erdogan F., "A surface crack in a graded medium loaded by a sliding rigid stamp", ***Engineering Fracture Mechanics***, 69:1729-1751, (2002).

[18] Ke L.L. and Wang Y.S., "Two-dimensional contact mechanics of functionally graded materials with arbitrary variations of material properties", ***International Journal of Solids and Structures***, 43: 5779-5798, (2006).

[19] Ke L.L. and Wang Y.S., "Two-dimensional sliding frictional contact of functionally graded materials", ***European Journal of Mechanics-A/Solids***, 26: 171-188, (2007).

[20] Shi X., Adachi A., Kida K., "Subsurface stress distribution and failure of PPS thrust bearings under rolling contact fatigue in water", ***Key Engineering Materials***, 814: 152-156, (2019).

[21] Liu J., Li X., Shi Z., "An investigation of contact characteristics of a roller bearing with a subsurface crack", ***Engineering Failure Analysis***, 116: 104744, (2020).

[22] Elsharkawy A.A., "Effect of friction on subsurface stresses in sliding line contact of multilayered elastic solids", ***International Journal of Solids and Structures***, 36: 3903-3915, (1999).

[23] Chidlow S.J., Teodorescu M., Vaughan N.D., "A solution method for the sub-surface stresses and local deflection of a semi-infinite inhomogeneous elastic medium", ***Applied Mathematical Modelling***, 36: 3486-3501, (2012).

[24] Savolainen M. and Lehtovaara A., "An approach to investigating subsurface fatigue in a rolling/sliding contact", ***International Journal of Fatigue***, 117: 180-188, (2018).

[25] Ali F., "Numerical study on subsurface stress in Hertzian contacts under pure sliding conditions", ***Journal of Applied and Computational Mechanics***, 6(SI): 1098-1106, (2020).

[26] Arslan O., "Computational contact mechanics analysis of laterally graded orthotropic half-planes", ***World Journal of Engineering***, 14/2: 145-154, (2017).

[27] Liu J., Ke L.L, Wang Y.S., "Two-dimensional thermoelastic contact problem of functionally graded materials involving frictional heating", ***International Journal of Solids and Structures***, 48(18): 2536-2548, (2011).

[28] Chen P. and Chen S., "Thermo mechanical contact behavior of a finite graded layer under a sliding punch with heat generation", ***International Journal of Solids and Structures***, 50(7-8): 1108-1119, (2013).

[29] Barik S.P., Kanoria, M., Chaudhuri P.A., "Steady state thermoelastic contact problem in a functionally graded material", ***International Journal of Engineering Science***, 46: 775-789, (2005).

[30] Choi H.J. and Paulino G.H., "Thermoelastic contact mechanics for a flat punch sliding over a graded coating/substrate system with frictional heat generation", ***Journal of the Mechanics and Physics of Solids***, 56: 1673-1692, (2008).

[31] Chen Y.C., Lee S.Y., "Elastic-Plastic Wheel -Rail Thermal Contact on Corrugated Rails During Wheel Braking", ***Journal of Tribology***, 131: 011401-1, (2009).

[32] Wu Y., Wei Y., Liu Y., Duan Z., Wang L., "3-D analysis of thermal-mechanical behavior of wheel/rail sliding contact considering temperature characteristics of materials", ***Applied Thermal Engineering***, 115: 455-462, (2017).

[33] Balci M.N., Dag S., Yildirim B., "Subsurface stresses in graded coatings subjected to frictional contact with heat generation", ***Journal of Thermal Stresses***, 40(4): 517-534, (2017).

[34] Balci M.N., Yildirim B., Dag S., "Analysis of frictional contacts with heat generation considering temperature dependent properties", ***International Journal of Mechanical Sciences***, 101-102: 59-69, (2015).

[35] Ling F.F., "Surface Mechanics", New York, ***John Wiley & Sons***, (1973).

[36] Watremetz B., Baietto-Dubourg M.C., Ulbricht A.A., "2D thermo-mechanical contact simulations in a functionally graded material: A multigrid-based approach", ***Tribology International***, 40: 754-762, (2007).

[37] ANSYS Inc., ***ANSYS Mechanical APDL Theory Reference***, v17.1, (2016).

[38] Apatay T., Dag S., Guler M.A., Gulgeç M., "Subsurface contact stresses in functionally graded coatings loaded by a frictional flat stamp", ***Journal of the Faculty of Engineering and Architecture of Gazi University***, 25(3): 611-623, (2010).

[39] Ootao Y., Tanigawa Y., Nakamura T., "Optimization of material composition of FGM hollow circular cylinder under thermal loading: a neural network approach", ***Composites Part-B***, 30: 415-422, (1999)